IEEE Photonics Journal
An IEEE Photonics Society Publication

Open Access

Period-Wise Phase Unwrapping Method With Two Gray Level Coding Patterns

Volume 13, Number 2, April 2021

Bolin Cai
Dongdong Xi
Lu Liu
Xiangcheng Chen
Yuwei Wang

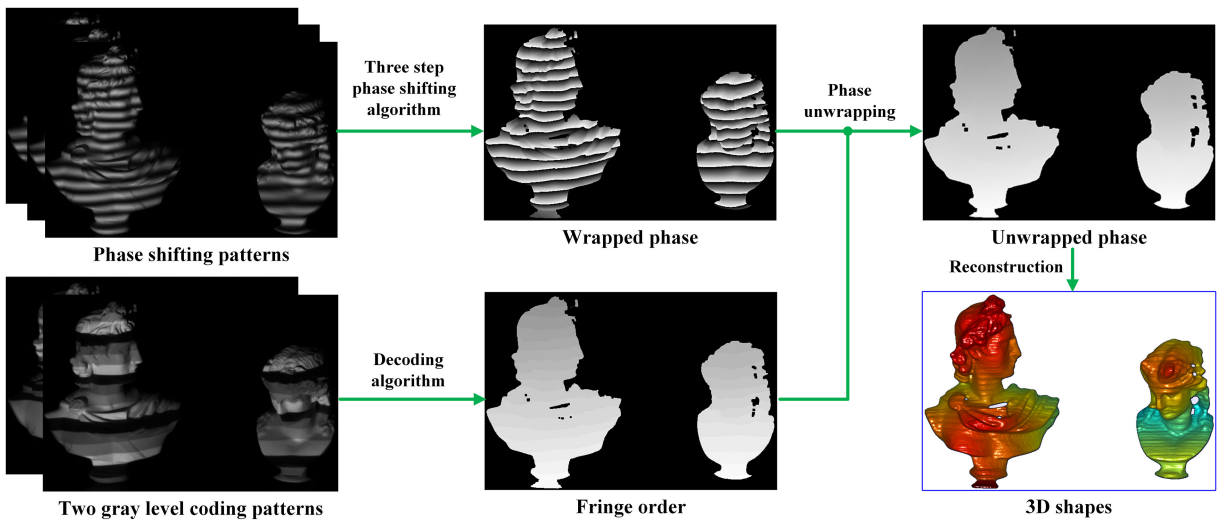

DOI: 10.1109/JPHOT.2021.3069123

Period-Wise Phase Unwrapping Method With Two Gray Level Coding Patterns

Bolin Cai,[1] **Dongdong Xi**,[2] **Lu Liu**,[2] **Xiangcheng Chen**,[3] **and Yuwei Wang**[2]

[1]National Engineering Research Center for Agro-Ecological Big Data Analysis and Application, Anhui University, Hefei 230601, China
[2]College of Engineering, Anhui Agricultural University, Hefei 230036, China
[3]School of Automation, Wuhan University of Technology, Wuhan 430070, China

DOI:10.1109/JPHOT.2021.3069123

Manuscript received February 10, 2021; revised March 22, 2021; accepted March 23, 2021. Date of publication March 26, 2021; date of current version April 20, 2021. This work was supported in part by the National Natural Foundation of China under Grants 51909005 and 61935008, in part by the Natural Science Foundation of Anhui Province under Grant 2008085QF318, and in part by the Graduate Innovation Found of Anhui Agricultural University under Grant 2021yjs-47. Corresponding author: Yuwei Wang (e-mail: wyw@ahau.edu.cn).

Abstract: Fringe projection profilometry is a widely used three-dimensional (3D) optical measurement technique. However, it is quite challenging to quickly obtain the 3D information of objects. Minimizing the number of patterns for phase unwrapping is an efficient way to address the above problem, and many methods have been proposed. This paper reports a period-wise phase unwrapping method with only two gray level coding patterns. Due to a hybrid coding strategy implemented, the number of patterns used in the proposed method reduces by one in comparison with conventional gray level method when generating the same number of codewords. A robust decoding scheme is also developed to determine the fringe order, and its accuracy is guaranteed by using the self-correcting method to remove the phase errors. Some experiments have been conducted, and their results confirm that the success of the proposed method.

Index Terms: Fringe projection, phase unwrapping, gray-level coding, fringe order.

1. Introduction

Fringe projection profilometry (FPP), as an optical non-contact measurement technique, has attracted much attention from scholars and been used in various fields because of its advantages of fast speed and high accuracy [1]–[3]. In this technique, the designed fringe patterns are projected onto an object, deformed patterns captured by a camera could be used to retrieve the phase information for reconstructing the three-dimensional (3D) geometry of the tested object. Generally, phase-shifting profilometry [4] and transform-based profilometry [5], [6] are the two main methods to recover phases at present. However, due to the arctangent function used in the two techniques, the phase is truncated at $[-\pi, \pi)$ [7]. To eliminate discontinuities and obtain the continuous phase map, a phase unwrapping operation is needed.

A variety of phase unwrapping algorithms have been proposed in recent decades, most of them can be roughly classified into spatial methods [8]–[10] and temporal methods [11], [12]. Spatial methods unwrap the phase by referring to the phase of its neighbor pixels from the same phase map. Obviously, the errors will be occurred when objects are under occlusion or discontinuity, and

propagate through the path. On the contrary, temporal methods recover the fringe order and the absolute phase parallelly with the assistance from additional projected patterns. Those methods usually possess high precision and high robustness even for objects containing a complex (e.g., discontinuous or isolated) surface. Hence researchers prefer the temporal methods, and have proposed a number of coding strategies including multiple-frequency [13], phase-coding [14]–[16], and binary coding or gray code [17]–[19]. The above three strategies have different coding domains, which are the frequency domain, the phase domain and the image gray domain, respectively. They all have excellent performance in 3D measurements, but require three or more coding patterns, making them unsuitable for dynamic measurement.

To overcome the above limitation, many new temporal methods have been proposed to reduce the number of used patterns in different coding domains, thus improving the acquisition speed. In the frequency domain, the two-frequency method, which only projects two sets of phase-shifting fringe patterns, requires six patterns to reconstruct 3D surfaces of objects [20]. With the assumption that the average intensities of the two sets are the same, a composite dual-frequency method only requires five patterns [21]. Nevertheless, to achieve high accuracy results, more than two types of frequencies are typically applied, which is time-consuming. For the phase domain, Wang *et al.* [14] presented a novel method embedding the order information into the absolute phase domain. The method is less sensitive to surface contrast, ambient light, and camera noise, but it also requires six designed patterns. After that, an approach embedding the codeword into the shifting phase is proposed [22]. The fringe order is innovatively coded into shifting phase, and it requires only sinusoidal patterns to recover the phase map. However, due to the phase range, the number of coded codewords is limited, thus the measurement results are unavailable when many codewords are required [23]. At last, the binary coding is a simple and widely used technique that encodes the fringe order into a sequence of binary patterns with different values in the image gray domain. The technique is more robust in comparison with the above methods. Binary coding methods including simple coding [17] and gray code [19] at least require $\log_2^M$patterns to generate M codewords, which are inefficient in time-critical measurements. To this end, Zheng *et al.* [24] used three intensity levels to develop a ternary gray-code method, and it needs $\log_3^M$ patterns to generate M periods. Subsequently, He *et al.* [25] proposed a quaternary gray-code method to further reduce the number of patterns. For simple binary coding, scholars proposed n-ary gray level methods to improve the measuring speed [26]. In conclusion, those binary coding algorithms have a common idea that encode $n > 2$ intensity levels effectively to reduce the required patterns from $ceil(\log_2^M)$ to $ceil(\log_n^M)$ for a wrapped phase with M periods. Assuming the $M = 64$, the above methods at least need three patterns for phase unwrapping, and totally six patterns for one measurement.

To further reduce the number of image gray coding patterns, this paper proposes a period-wise phase unwrapping method to generate at least 64 codewords with only 2 gray level patterns. The proposed method encodes the fringe order into two gray level patterns. Moreover, for the different coding patterns, we use different code sequences and the coding period is also different, thus the coding strategy is named hybrid coding strategy (HCS). Among the two coding patterns, one gray level pattern is used to determine the local order for each pixel, the other can locate the region order for several adjacent fringe periods. Thus, every fringe period can be distinguished. To make the proposed method more robust and flexible, we also implemented a self-correcting algorithm to remove the errors caused by the ambient light and noise. Experiment results have demonstrated the performance of the proposed method.

2. Principles

2.1 Conventional Gray Level (CGL) Coding Method

The CGL method needs two sets of fringes for 3D surface measurements. One set consists of phase-shifting patterns utilized for wrapped phase calculation, while the other set consists of gray level coding patterns applied for fringe order recovery [27], [28]. Since the three-step phase-shifting algorithm requires the least number of patterns to compute the phase map, we choose the

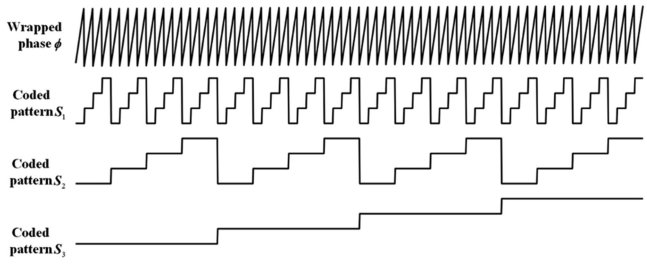

Fig. 1. Coding strategy of the CGL method.

three-step phase-shifting algorithm in this paper. The intensities of phase-shifting patterns can be expressed as:

$$I_n(x, y) = a(x, y) + b(x, y)\cos[\phi(x, y) + \delta_n] \tag{1}$$

here $n = 1, 2, 3$; $a(x, y)$ denote the background, $b(x, y)$ is the intensity modulation; $(x, y)$is the image coordinate, $\delta_n$is the step shift, and δ_1=$-2\pi/3$, δ_2=0, δ_3=$2\pi/3$; $\phi(x, y)$is the phase to be retrieved, and can be calculated by the following [29]:

$$\phi(x, y) = \tan^{-1}[\sqrt{3}(I_1 - I_3)\Big/(2I_2 - I_1 - I_3)] \tag{2}$$

Solving following two equations, the $a(x, y)$ and $b(x, y)$ can be obtained:

$$a(x, y) = (I_1 + I_2 + I_3)/3 \tag{3}$$

$$b(x, y) = \sqrt{3(I_1 - I_3)^2 + (2I_2 - I_1 - I_3)^2}\Big/3 \tag{4}$$

As mentioned above, the CGL method encodes n $>$ 2 intensity levels to determine the fringe order. Specifically, the number of gray level coding patterns is three, and each pattern has a different period. Since increasing the intensity level will result in code detection errors, and fringes with 64 periods are enough for general measurement, we employ n =4 to generate gray level coding patterns. The code sequence CS is "1234", three coded patterns can be written as

$$S_m(x, y) = a(x, y) + b(x, y)\left\{\frac{2CS[ceil(M/4)]}{3} - \frac{5}{3}\right\}, \text{ with } M = ceil(x/T_m) \tag{5}$$

where $m = 1, 2, 3$; $ceil(i)$ rounds the elements of i to the nearest integers towards infinity; $a(x, y)$ and $b(x, y)$ is the same as $a(x, y)$ and $b(x, y)$ appeared in the Eq. (1); $CS(i)(i = 1, 2, 3, 4)$ is the j-th codes in CS; T_m is the period of coded pattern S_m. Assuming the period of the sinusoidal pattern is T , as shown in Fig. 1, the relationship of T_1, T_2 and T_3 is $T_3 = 4T_2 = 16T_1 = 16T$. The flowchart of the CGL method is shown in Fig. 2.

Once those patterns are captured, the $a(x, y)$ and $b(x, y)$ calculated by Eqs. (3)–(4) can be utilized to normalize coded patterns, and then three code maps can be calculated:

$$S'_m(x, y) = \frac{(S_m(x, y) - a(x, y))}{b(x, y)} \tag{6}$$

$$C_{sm}(x, y) = round\left(\frac{3}{2}S'_m + \frac{5}{2}\right) \tag{7}$$

here m = 12,3. Code maps C_{s1} , C_{s2} and C_{s3} are employed to determine the fringe order:

$$K(x, y) = 16C_{s3}(x, y) + 4C_{s2}(x, y) + C_{s1}(x, y) - 20 \tag{8}$$

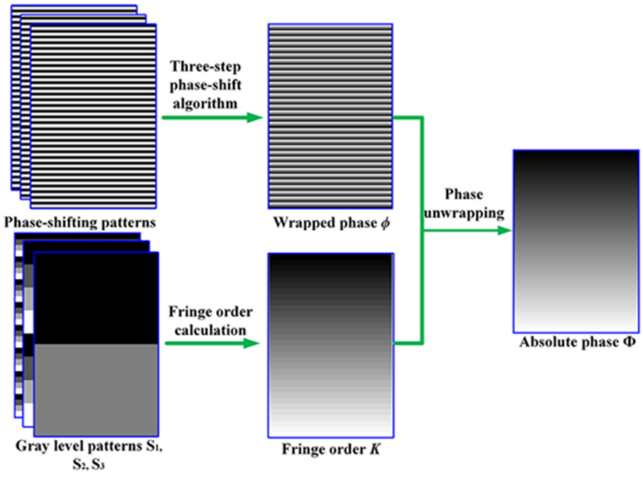

Fig. 2. Flowchart of the CGL method.

TABLE 1
Two Code Sequences CS_1 and CS_2

CS_1	1	1	1	1	1	1	1	1	1	1	1	1	1	1	1	1	2	2	2	2	2	2	2	2	2	2	2	2	2	2
CS_2	1	1	1	1	2	2	2	2	3	3	3	3	4	4	4	4	2	2	2	2	3	3	3	3	4	4	4	4	1	1	1	1
CS_1	3	3	3	3	3	3	3	3	3	3	3	3	3	3	3	3	4	4	4	4	4	4	4	4	4	4	4	4	4	4	4	4
CS_2	3	3	3	3	4	4	4	4	1	1	1	1	2	2	2	2	4	4	4	4	3	3	3	3	2	2	2	2	1	1	1	1

Finally, the unwrapped phase $\Phi(x, y)$ can be recovered by the wrapped phase $\phi(x, y)$ and the fringe order $K(x, y)$:

$$\Phi(x, y) = \phi(x, y) + 2\pi \times K(x, y) \tag{9}$$

2.2 Period-wise Gray Level (PWGL) Coding Method

As mentioned above, the CGL still needs six patterns for phase unwrapping. To further reduce the number of the coded patterns, a period-wise gray level coding method is presented in this work. Compared with the CGL method, the proposed method only requires two patterns when encoding the same number of codewords.

2.2.1 Details of PWGL Method: To generate the same 64 codewords, we also set n = 4 to describe the proposed method. One of the two gray level coding patterns G_1, which used to determine the local order K_1, is the same as S_1 that used in CGL. The other gray level coding pattern G_2 is encoded particularly, and utilized to calculate the region order K_2. Each period of the pattern G_2 is divided into two equal parts, and the two parts are encoded using different code sequences. Two specific code sequences CS_1 and CS_2 are illustrated in Table 1. Both CS_1 and CS_2 contain 64 codewords. Specifically, the CS_1 encodes the first parts of G_2, and the second parts of G_2 are coded using the sequence CS_2. Using the two code sequences, G_2 is mathematically expressed as:

$$G_2(x, y) = \begin{cases} A + B\left\{\frac{2CS_1[ceil(x/T)]}{3} - \frac{5}{3}\right\}, \mathrm{mod}(x, T) \le T/2 \\ A + B\left\{\frac{2CS_2[ceil(x/T)]}{3} - \frac{5}{3}\right\}, \mathrm{mod}(x, T) > T/2 \end{cases} \tag{10}$$

where $\mathrm{mod}(m, n)$ returns the remainder after division of m by n; $CS_1(i)$or $CS_2(i)$ represents the i-th code in CS_1 or CS_2. $ceil(m)$ rounds the elements of m to the nearest integers towards infinity. 2-bit

TABLE 2
The Corresponding Relationship Between K_2 and 2-bit Codewords C_1C_2

C_1 C_2	1 1	1 2	1 3	1 4	2 2	2 3	2 4	2 1
K_2	0	4	8	12	16	20	24	28
C_1 C_2	3 3	3 4	3 1	3 2	4 4	4 3	4 2	4 1
K_2	32	36	40	44	48	52	56	60

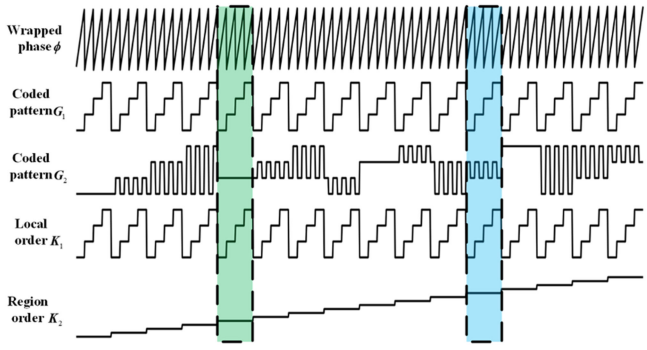

Fig. 3. Coding strategy of the PWGL method.

codewords C_1C_2 can be recovered from the pattern G_2, and the corresponding relationship between the order K_2 and C_1C_2 is shown in Table 2. Therefore, the region order is directly determined by the pattern G_2. Obviously, for each period of G_2, its order can be determined by the codewords combining the code of its first part with its second part, and can be computed as:

$$K_2 = \begin{cases} (C_1 - 1) * 16 + (C_2 - C_1) * 4, C_2 \geq C_1 \\ (C_1 - 1) * 16 + (C_2 - C_1 + 4) * 4, C_2 < C_1 \end{cases} \tag{11}$$

Fig. 3 shows the details of coding strategy used in the PWGL method, and its corresponding orders. Exactly, in HCS, the order of one fringe period is determined by codewords from different code sequences. As can be seen from Fig. 3, the two regions in green and blue have four consecutive periods, and each period corresponds to a same 2-bit codewords. In other words, one K_2 corresponds to four fringe period. So, we call K_2 the region order. The coded map computed from G_1 using Eqs. (6)–(7) can be directly regarded as the local order K_1. Then the fringe order K can be calculated as:

$$K = K_1 + K_2 \tag{12}$$

Smooth absolute phase map can be obtained using the Eq. (9). The details of the proposed method are shown in Fig. 4.

2.2.2 Decoding Algorithm: To obtain the accurate fringe order, a decoding algorithm is presented in this paper. Specifically, the main purpose of the algorithm is to determine the region order K_2 because the local order K_1 is easily obtained as described in Section 2.2. The algorithm includes two vital procedures: code detection and region order determination. The principle of the proposed algorithm is illustrated in Fig. 5.

2.2.2.1 Code detection: As we know, a fringe can be exactly split into many parts with aid of the phase values. In this paper, a phase value 0 is selected to divide the fringe into two parts since the wrapped phase ranges $[-\pi, \pi)$. In other words, the period of C_1 and C_2 is half that of the fringe. For each fringe period, it contains two different codes, which can affect each other and induce

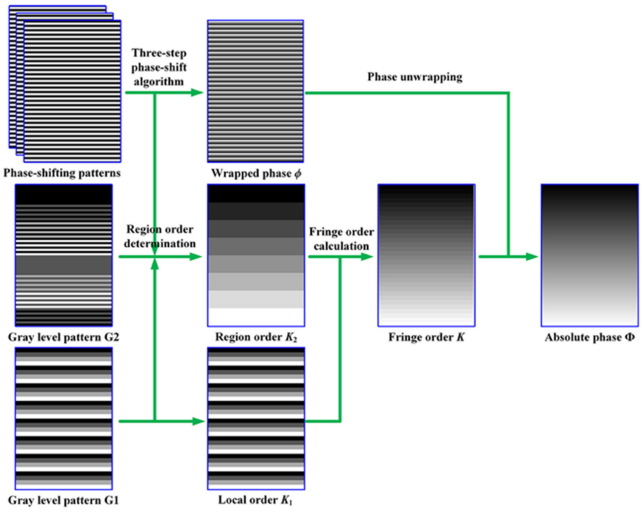

Fig. 4. Flowchart of the PWGL method.

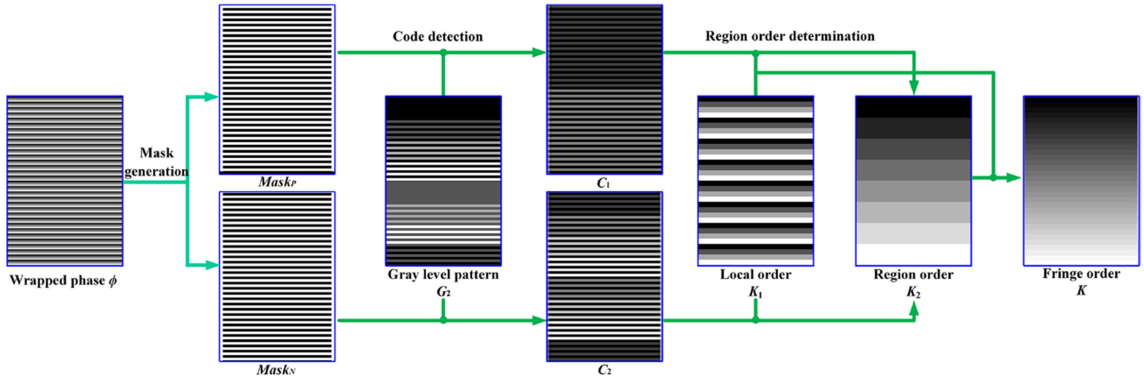

Fig. 5. The principle of the proposed decoding algorithm.

incorrect codes. Therefore, an accurate code detection operation based on phase segmentation is employed. Firstly, two binary masks can be obtained:

$$Mask_P(x, y) = \begin{cases} 1, & \text{if } \phi(x, y) > 0 \\ 0, & \text{if } \phi(x, y) \leq 0 \end{cases}$$
$$Mask_N(x, y) = \begin{cases} 0, & \text{if } \phi(x, y) > 0 \\ 1, & \text{if } \phi(x, y) \leq 0 \end{cases} \quad (13)$$

Then, we use the Eq. (6) to normalize G_2 to obtain a code map C_{map}. The map is multiplied with $Mask_N(x, y)$ and $Mask_P(x, y)$ to obtain C_1 and C_2, respectively. By labeling connected regions of the two masks, we can distinguish each code of C_1 and C_2. The mean normalized intensity of every code is computed and employed to refine a correct code. This step detects and corrects the code one by one based on the characteristics of phase distribution, and lays the foundation for region order determination. The details of the self-correcting algorithm can be seen in our previous work [30].

2.2.2.2 Region order determination: Region order calculation need the information provided by not only C_1 and C_2, but also the local order K_1. The local order is calculated using the pattern G_1 and corrected using the algorithm as described above. Therefore, all the information which utilized

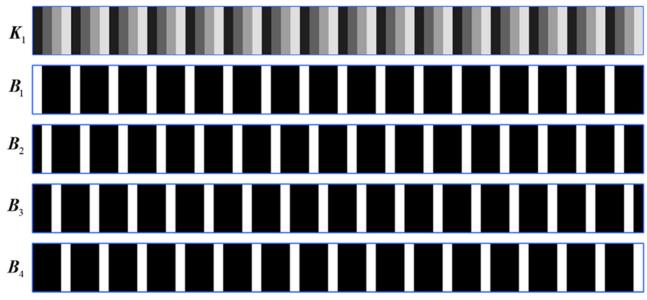

Fig. 6. Masks generated by using the local order K_1.

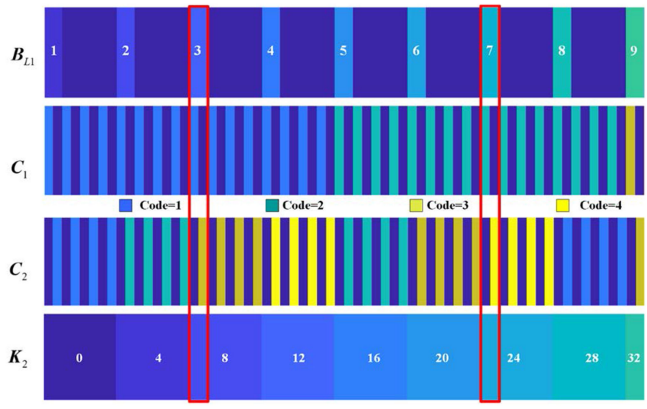

Fig. 7. Determination of region orders.

to recover K_2 has been preprocessed to guarantee the accuracy. Since the period of K_1 is the same as that of the fringe, we can use it to match C_1 and C_2 one by one correctly. Then we use the two matched codes to get their corresponding region order. The detail steps of the region order determination are as follows:

Step1: Regions generation and labeling. In the case without risk of confusion, we take the vertical stripe for an example for brevity. The code values of K_1 are used to generate four binary masks, as shown in Fig. 6.

$$B_i(x, y) = \begin{cases} 1, & \text{if } K_1(x, y) = i \\ 0, & \text{otherwise} \end{cases} \text{where} i = 1, 2, 3, 4 \tag{14}$$

Obviously, the four masks can locate all the regions with different codes, and regions with a same code distribute in one mask. After the labeling operation, every region within same mask can be marked with a unique integer values greater than 0, and the background are labeled 0. Thus, all the fringes can be period-wise extracted and determined one by one.

Step2: Decoding complete stripes. The labeled masks can be used to extract the code C_1 and C_2, then the region order is determined. We take the B_1 as an example, its labeled graphic is B_{L1}, and the number of its connected regions is Num. When decoding the stripe corresponding to *j-th* ($j = 12{,}3 \ldots Num$) region, we can exploit the region to extract the C_1 and C_2 that are respective to the same stripe. Once the codes are determined, the region order can be computed using Eq. (11). As shown in Fig. 7, this is one part of the B_{L1}. Two regions circled by red rectangle are labeled 3 and 7, respectively. The corresponding codes of the first region in C_1 and C_2 are 1 and 3, respectively. Therefore,

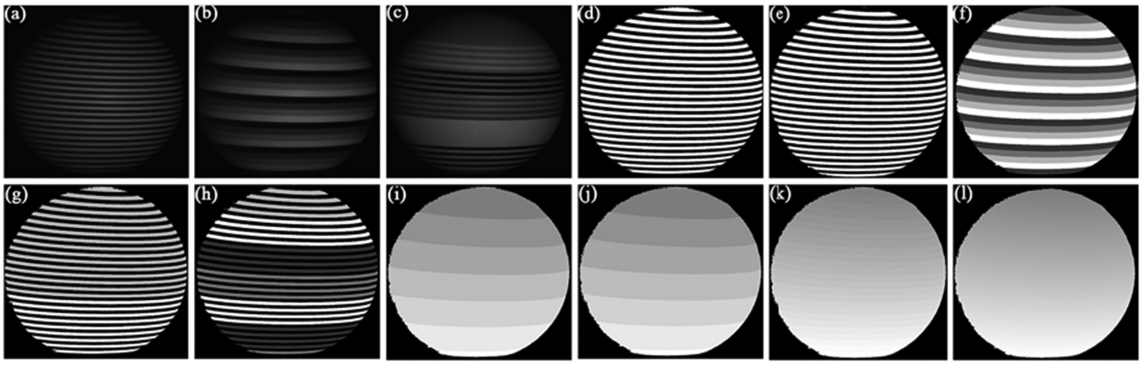

Fig. 8. The ball. (a)–(c) Some deformed images; (d)–(e) two masks obtained using the wrapped phase; (f) the local order K_1; (g)–(h) code C_1 and C_2; (i) the incomplete region order; (j) the region order K_2; (k) the fringe order; (l) the absolute phase.

the region order of the stripe which corresponding to this region is 8. Two codes of the second region are 2 and 4, and its region order is 24.

Step3: Order determination with one code losing. In the practical measurements, objects usually do not occupy the entire frame of the image, thus the deformed fringes may be partially missing and incomplete stripes are inevitable. That is to say, either C_1 or C_2 may lose, especially in edge regions. As for such cases, the approach described in step 2 is failed, but its region order can be determined by referring to their adjacent periods. Clearly, the situation that both C_1 and C_2 are lost is impossible. Hence, we only need to consider cases that one code loses. When C_1 of current period is lost, we can use the region order K_2^{next} of the next stripe to calculate its region order. If local order of current period is 1, the region order is $K_2 = K_2^{next}$. If local order of current period is other value, the region order is $K_2 = K_2^{next} - 4$. Similarly, when C_2 of current period is lost, we firstly computed its local order and the region order K_2^{pre} of the precious stripe. If local order of current period is 4, the region order is $K_2 = K_2^{pre}$. If local order of current period is other value, the region order is $K_2 = K_2^{pre} + 4$.

Once the decoding operations are done, the local order K_1 and the region order K_2 are determined precisely. Then the fringe order can be calculated using Eq. (12).

3. Results

To verify the performance of the PWGL method, an FPP system consisting of a camera (Point Grey Chameleon3) and a projector (DLP Light Crafter 4500) has been set up. The resolution of the camera and the projector are 1280 $\times$ 1024 pixels and 912 $\times$ 1140 pixels, respectively.

3.1 Comparison Experiments

To verify the reliability of the PWGL method, we firstly measured a ball using the PWGL method, the correction method described in Ref. [30] and the CGL method. The 12-step phase-shifting patterns are also projected on the ball, and the absolute phase map calculated by the 12-step phase-shifting algorithm is used as the ideal reference ground truth. In experiments, the period of the sinusoidal fringe is 20 pixels. Some of captured images of the PWGL method are shown in Fig. 8(a)–(c). The details of processing process of the propose method are shown in Fig. 8(d)–(l). Firstly, two masks, as shown in Fig. 6(d) –(e), generated by the wrapped phase are used to detect the C_1 and C_2. Then, using the information of K_1, we can determine two codes corresponding to one stripe period, and then calculate the region order K_2. The map which only contains the order information of complete

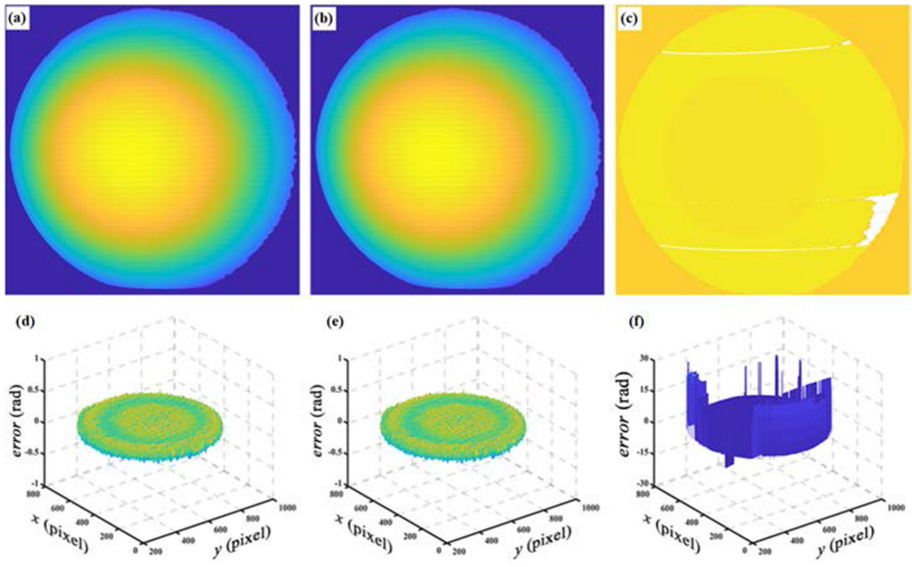

Fig. 9. Results of the ball. (a)–(c) Reconstructed results by using the PWGL, the Ref. [30] and the CGL method, respectively; (d)–(f) three error distribution maps corresponding to (a)–(c), respectively (unit: rad).

stripes is so called the incomplete region order, as shown in Fig. 6(i). After we obtained the region order of some incomplete stripes, the accurate region order is finally determined. The fringe order and the wrapped phase are shown in Fig. 6(k)–(l), respectively.

Meanwhile, we reconstructed the 3D shapes of the ball by using the CGL method and the correction method described in Ref. [30]. Reconstructed results obtained by the PWGL method, the [Ref. [30] and the CGL method are shown in Fig. 9(a)–(c), respectively. Referring the real value obtained by the 12-step phase-shifting algorithm, three error distribution maps can be obtained, shown in Fig. 9(d)–(f). Obviously, errors obtained by the PWGL method and the [Ref. [30] are small and their distribution are uniform. However, the distribution map of the CGL method has abrupt changes, and the measuring result is unavailable. The sensitivity to noises of the CGL method is also proved by the measuring result. The root mean square errors (RMSEs) of the 3D reconstructions are 0.2437 rad for PWGL method, 0.2438 rad for the [Ref. [30] and 4.3641 rad for CGL method, proving that the PWGL method has comparable accuracy with the [Ref. [28] and has higher measurement accuracy than the CGL method. It is important to point out that the PWGL method achieve the accurate measurement with fewer coded patterns in comparison with another two methods.

3.2 Verification Experiments

To verify the performance of the PWGL method, we projected designed patterns on objects with complex surfaces. We firstly measure a single sculpture, the deformed images of the PWGL method are shown in Fig. 10(a)–(c). The two gray level coding patterns were binarized using Eq. (6), and the wrapped phase can be obtained. Figs 10(d) and (e) show two mask maps obtained from the wrapped phase, the two masks can be employed to correct the local order K_1 and detect the C_1 and C_2, as shown in Fig. 10(f)–(h). By use of four binary masks generated by the K_1, we can determine two codes that corresponding to a same complete stripe. Then, the region order of complete stripes are distinguished, as illustrated in Fig. 8(i). While for those stripes that missing one code because of the shape of objects, its region order can be determined with assist of the region order information of its adjacent stripes. Fig. 10(j) shows the region order of all the stripes. Once the decoding

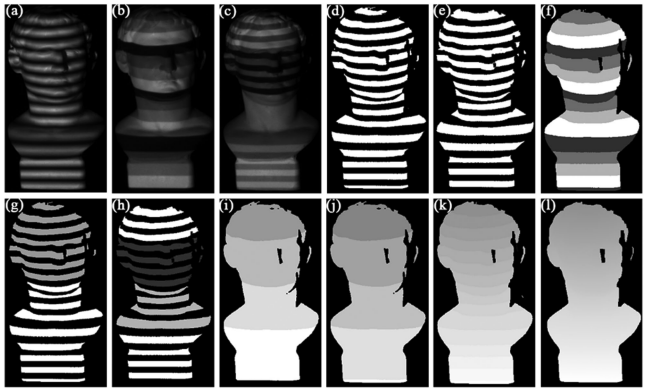

Fig. 10. The single sculpture. (a)–(c) Some deformed images; (d)–(e) two masks obtained using the wrapped phase; (f) the local order K_1; (g)–(h) code C_1 and C_2; (i) the incomplete region order; (j) the region order K_2; (k) the fringe order; (l) the absolute phase.

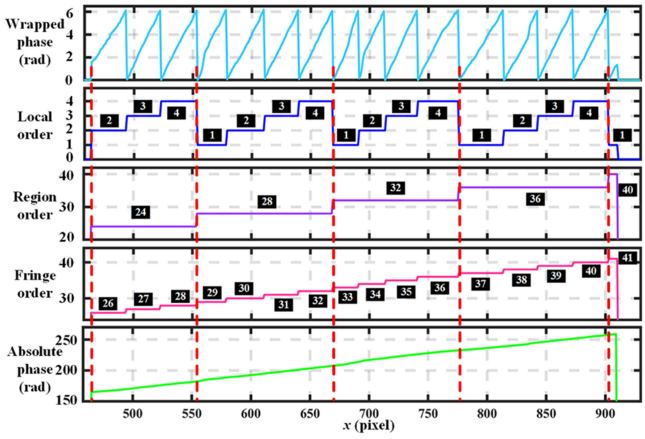

Fig. 11. 530th column cross sections of the wrapped phase, K_1, K_2, the fringe order and the absolute phase of the sculpture.

operation is done, the accurate region order is determined. Using the Eq. (12), the fringe order can be recovered, as shown in Fig. 10(k). Finally, the unwrapped phase is obtained. As can be seen in Fig. 11, 530th column cross sections of the wrapped phase, K_1, K_2, the fringe order and the absolute phase are plotted. Obviously, the wrapped phase ϕ and K_1 are aligned well with every period, and one region order corresponds to four period stripes. The smooth cross section of the absolute phase indicates the success of our method. Moreover, we recovered the 3D surfaces of the single sculpture by using the PWGL and CGL methods at the same time. The results are shown in Fig. 12. Apparently, due to the noises, result obtained by the CGL method is unavailable. The PWGL method can recover the smooth surface, and the details show well. This experiment definitely demonstrates that our method has a better performance than the CGL method.

Furthermore, two isolated sculptures were reconstructed to demonstrate the effectiveness of the PWGL method. We employed the algorithm described in this paper to address the fringe order and unwrap the phase. Figs 13(a)–(c) show the deformed images. The wrapped phase is Fig. 13(d). Then, the proposed decoding algorithm is employed to calculate the fringe order. The local order K_1, the region order K_2, the fringe order K, and absolute phase are shown in Fig. 13(e)–(h), respectively. Fig. 14 shows the 3D reconstruction results of the two isolated objects calculated by the CGL and PWGL methods. Similarly, the surface obtained by the PWGL method is smooth and the details

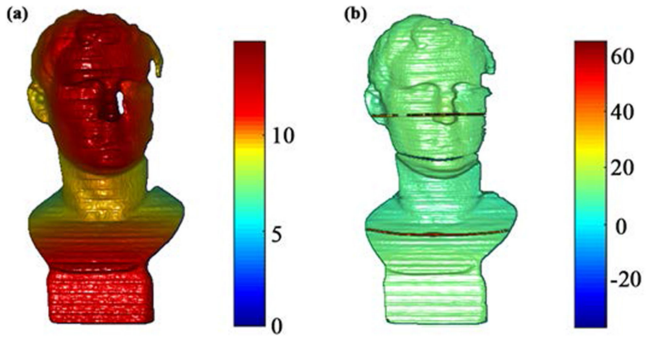

Fig. 12. Reconstructed results. (a)–(b) results recovered by using the PWGL and CGL method, respectively (unit rad).

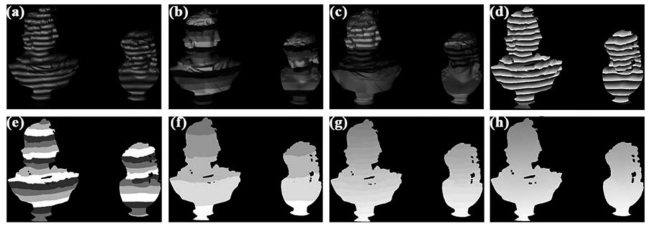

Fig. 13. Two isolated sculptures. (a)–(c) Some deformed images; (d) the wrapped phase; (e) the local order K_1; (f) the region order K_2; (g) the fringe order; (h) the absolute phase.

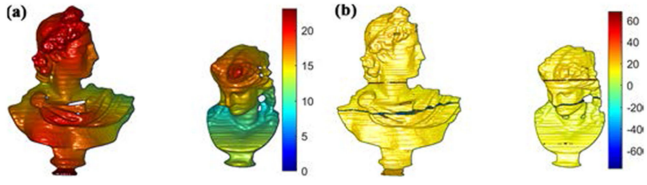

Fig. 14. Reconstructed results. (a)–(b) results recovered by using the PWGL and CGL method, respectively (unit rad).

appear well. There are many obvious errors on the surfaces obtained by the CGL method. The results of the above two experiments definitely prove that the PWGL method is a success in measuring objects with complex surfaces.

4. Discussions

The PWGL method can determine at least 64 fringe order using only 2 gray level coding patterns. Two different coding sequences are employed to encode fringe order information. We also proposed a period wise decoding algorithm to distinguish the order. Compared with other image gray domain coding methods, we discuss the proposed method with the following aspects:

4.1 The Number of Codewords

Benefit from the proposed coding strategy, the PWGL method can generate a large number of codewords with only two patterns. Zheng's method [19] and He's method [20] encode the order information into image gray domain with $n = 3$ and $n = 4$, respectively. Thus, if M^3 codewords are generated, Zheng's method [19] and He's method [20] need $ceil(3\log_3^M)$ and $ceil(3\log_4^M)$ coded

patterns, respectively. For the CGL method, it needs 3 coded patterns, and the image gray should be divided into M levels. However, the PWGL method only needs 2 patterns to generate M^3 codewords. Obviously, the proposed method has the advantage of generating more codewords with only 2 patterns. It has the potential in dynamic measurements.

4.2 Measuring Speed

Additionally, compared with the CGL method, the coding strategy proposed in our method is complex, such that it costs more time to recover the accurate fringe order. This limitation certainly can be solved using high performance hardware processors. A graphics processing unit (GPU) or a field-programmable gate array (FPGA) is alternative. The dithering technique is also can be used to reduce the measurement time. Although the PWGL method is not trouble free, it exactly enhances the measurement speed for 3D measurement using binary coding category.

4.3 Measurement Limits

The decoding algorithm is working on the assumption that objects surfaces are smooth enough, thus the adjacent fringes are independent with no offset intersection. Once objects with some large and abrupt changes, the adjacent stripes may intersect with each other, and the codes cannot be distinguished accurately. But the PWGL method can be employed in most cases such as measuring regular geometric objects, objects with complex surfaces and two isolated objects. Moreover, this limitation could be addressed with neural network or deep learning.

5. Conclusion

A PWGL phase unwrapping method is introduced in this paper. Based on an HCS, two different codes are embedded into one fringe period. We also develop a detailed decoding algorithm to recover the accurate fringe order, and the performance of the method is therefore guaranteed. Compared with the CGL method, the proposed method uses fewer patterns to generate the same number of codewords, and possesses the preferable accuracy. Experiment results demonstrate the success of our method.

References

[1] Z. Wang, "Review of real-time three-dimensional shape measurement techniques," *Measurement*, vol. 156, 2020, Art. no. 107624.
[2] S. Zhang, "Absolute phase retrieval methods for digital fringe projection profilometry: A review," *Opt. Lasers Eng.*, vol. 107, pp. 28–37, 2018.
[3] J. Xu and S. Zhang, "Status, challenges, and future perspectives of fringe projection profilometry," *Opt. Lasers Eng.*, vol. 135, 2020, Art. no. 106193.
[4] C. Zuo, S. Feng, L. Huang, T. Tao, W. Yin, and Q. Chen, "Phase shifting algorithms for fringe projection profilometry: A review," *Opt. Lasers Eng.*, vol. 109, pp. 23–59, 2018.
[5] M. Takeda and K. Mutoh, "Fourier transform profilometry for the automatic measurement of 3-D object shapes," *Appl. Opt.*, vol. 22, pp. 3977–3982, 1983.
[6] J. Zhong and J. Weng, "Spatial carrier-fringe pattern analysis by means of wavelet transform: Wavelet transform profilometry," *Appl. Opt.*, vol. 43, pp. 4993–4998, 2004.
[7] Y. Wang *et al.*, "Spatial binary coding method for stripe-wise phase unwrapping," *Appl. Opt.*, vol. 59, pp. 4279–4285, 2020.
[8] G. Jian, "Reliability-map-guided phase unwrapping method," *IEEE Trans. Geosci. Remote Sens. Lett.*, vol. 13, no. 5, pp. 716–720, May 2016.
[9] M. Zhao, L. Huang, Q. Zhang, X. Su, A. Asundi, and Q. Kemao, "Quality-guided phase unwrapping technique: Comparison of quality maps and guiding strategies," *Appl. Opt.*, vol. 50, pp. 6214–6224, 2011.
[10] Y. Lu, X. Wang, and X. Zhang, "Weighted least-squares phase unwrapping algorithm based on derivative variance correlation map," *Optik*, vol. 108, pp. 62–66, 2007.
[11] H. Yuan *et al.*, "Phase-shifting coding method for absolute phase retrieval," *Opt. Eng.*, vol. 58, no. 10, 2019, Art. no. 104103.
[12] Y. Chen *et al.*, "3D measurement method based on S-shaped segmental phase encoding," *Opt. Laser Technol.*, vol. 121, 2020, Art. no. 105781.

[13] Y. Hu *et al.*, "Microscopic 3D measurement of shiny surfaces based on a multi-frequency phase-shifting scheme," *Opt. Lasers Eng.*, vol. 122, pp. 1–7, 2019.
[14] Y. Wang and S. Zhang, "Novel phase-coding method for absolute phase retrieval," *Opt. Lett.*, vol. 37, pp. 2067–2069, 2012.
[15] X. Chen, Y. Wang, Y. Wang, M. Ma, and C. Zeng, "Quantized phase coding and connected region labeling for absolute phase retrieval," *Opt. Exp.*, vol. 24, pp. 28613–28624, 2016.
[16] Y. Wang *et al.*, "Enhanced phase-coding method for three-dimensional shape measurement with half-period codeword," *Appl. Opt.*, vol. 58, pp. 7359–7366, 2019.
[17] S. Zhang, "Flexible 3D shape measurement using projector defocusing: Extended measurement range," *Opt. Lett.*, vol. 35, pp. 934–936, 2010.
[18] Y. Wang, S. Zhang, and J. H. Oliver, "3D shape measurement technique for multiple rapidly moving objects," *Opt. Exp.*, vol. 19, pp. 8539–8545, 2011.
[19] D. Zheng *et al.*, "Phase-shifting profilometry combined with Gray-code patterns projection: Unwrapping error removal by an adaptive median filter," *Opt. Exp.*, vol. 25, no. 5, pp. 4700–4713, 2017.
[20] J. Li, H. Su, and X. Su, "Two-frequency grating used in phase-measuring profilometry," *Appl. Opt.*, vol. 36, pp. 277–280, 1997.
[21] K. Liu, Y. Wang, D. Lau, Q. Hao, and L. G. Hassebrook, "Dual-frequency pattern scheme for high-speed 3D shape measurement," *Opt. Exp.*, vol. 18, pp. 5229–5244, 2010.
[22] G. Wu *et al.*, "High-resolution few-pattern method for 3D optical measurement," *Opt. Lett.*, vol. 44, pp. 3602–3605, 2019.
[23] B. Cai *et al.*, "Absolute phase measurement with four patterns based on variant shifting phases," *Rev. Sci. Instrum.*, vol. 91, 2020, Art. no. 065115.
[24] D. Zheng, Q. Kemao, F. Da, and H. S. Seah, "Ternary gray code-based phase unwrapping for 3D measurement using binary patterns with projector defocusing," *Appl. Opt.*, vol. 56, pp. 3660–3665, 2017.
[25] X. He, D. Zheng, Q. Kemao, and G. Christopoulos, "Quaternary gray code phase unwrapping for binary fringe projection profilometry," *Opt. Lasers Eng.*, vol. 121, pp. 358–368, 2019.
[26] X. Chen *et al.*, "Modified gray-level coding method for absolute phase retrieval," *Sensors*, vol. 17, no. 10, 2017, Art. no. 2383.
[27] J. Geng. "Structured-light 3D surface imaging: A tutorial," *Adv. Opt. Photon.*, vol. 3, pp. 128–160, 2011.
[28] J. L. Posdamer and M. D. Altschuler. "Surface measurement by space-encoded projected beam systems," *Comput. Graph. Image Process.*, vol. 18, pp. 1–17, 1982.
[29] P. S. Huang and S. Zhang, "Fast three-step phase-shifting algorithm," *Appl. Opt.*, vol. 45, pp. 4503–4509, 2005.
[30] B. Cai *et al.*, "An improved gray-level coding method for absolute phase measurement based on half-period correction," *Opt. Lasers Eng.*, vol. 128, 2020, Art. no. 106012.